Variable Fidelity Optimization of Required Power of Rotor Blades: Investigation of Aerodynamic Models and their Application

Gunther Wilke
German Aerospace Center (DLR) Braunschweig, Institute of Aerodynamics and Flow Technology
Lilienthalplatz 7, 38108 Braunschweig, Germany, gunther.wilke@dlr.de

Abstract

An investigation of aerodynamic models with varying fidelity is performed with respect to the required power for different rotor blade geometries. Concluding from this investigation low, mid and high fidelity methods are selected. For hover these comprise a finite state inflow model, Euler computations on coarse meshes and highly resolved RANS computations, both with periodic boundaries. For forward flight, a prescribed wake model, single bladed Euler computations and a Chimera setup for RANS computations are selected. A comparative study between between single fidelity and variable fidelity surrogate based optimization is performed, where resource savings of up to 64.8% are seen for forward flight optimizations.

1 INTRODUCTION

The aerodynamic optimization of helicopter rotors is highly complex due the unsteady flow phenomena. In hover, the flow field is dominated by the blade vortices and the downwash of the previous blade, while in forward flight transonic effects and dynamic stall are added. The fluid-structure coupling is mandatory to account for the aero-elastic effects of the problem, requiring a great amount of computational power for the unsteady analysis and optimization of rotor blades. In his survey, Ganguli [14] depicts two routes for the optimization of rotor blades, either gradient based local optimization, or the application of genetic algorithms of global scope within surrogate models of the goal function.

The first route is taken by Le Pape and Beaumier [28], who use a gradient optimizer and a CFD solver to find new blade plan form shapes for a 7A and ERRATO blade. They compute the gradient using finite differences, while Choi et al. [32], as well as Dumont et al. [1] use the adjoint methodology to compute the gradient of the goal function more quickly.

The other route, surrogate based rotor optimization, is split into two major surrogate types, artificial neural networks and Kriging. Artificial neural networks are employed by Sajial et al. [19] to reduce the hub loads through a higher harmonic control device. Massaro et al. [4] apply a genetic algorithm to an artificial neural network to minimize the required power of a rotor using a lifting line model as well as a panel method coupled with a wake model. Performing high fidelity CFD computations, Johnson and Barakos [10] develop an optimization framework consisting of an artificial neural network and a genetic algorithm to optimize the pitching moments of a UH-60 blade in forward flight. Kriging, the other majorly used surrogate, is utilized by Glaz et al. [8] to reduce vibratory hub loads. They compute their aerodynamics using a rational function approach, which models the unsteady aerodynamics of rotors with flaps. Vu et al. [25] applies Kriging for the optimization of rotor airfoils of a BO-105 rotor computed with a 2D panel code. A combined aerodynamic, aero-acoustic, CFD oriented optimization is undertaken by Chae et al. [30] for a total of 19 design variables. Another high fidelity CFD optimization for a hover and a forward flight test case is carried out by Imiela [17].

A different surrogate based procedure is gone by Collins [9], who couples two surrogates models of variable fidelity (VF) together using response surface to quickly access the goal functions of vibratory hub loads and torque. He uses a lifting line model as well as hybrid CFD/wake coupled method for the simulation of the rotor aerodynamics.

This work continues Collins's idea, where the surrogate model is mostly created using low fidelity simulations, such as the blade element theory, and then calibrated with CFD data to yield high fidelity results. Recent approaches for variable fidelity surrogates are either Co-Kriging or Hierarchical Kriging. The first approach fuses high and low fidelity data together through a combined correlation matrix, while Hierarchical Kriging is based upon supplying the trend function from a low fidelity model instead of a polynomial function. Forrester et al. [3] as well as Yamazaki and Mavripilis [34] perform Co-Kriging based drag minimization of a wing and of a NACA0012 airfoil, respectively. The later also takes advantage of gradient information. Hierarchical Kriging is used by Han and Görtz [15] for aero-loads prediction, and Xiong et al. [33] show the application of it to surrogate based optimization for two synthetic and one engine piston problem.

The optimization performed in this paper focuses on Kriging based optimization of rotor blades using variable fidelity methods. The advantage of Kriging models over artificial neural networks is that they feature the metric of expected improvement. This metric takes

into account the goal function value, as well as the uncertainty of the model. Jones et al. [11] are the first to build a surrogate based optimization framework exploiting the expected improvement function, referred to as Efficient Global Optimization (EGO) algorithm.

Before this variable fidelity optimization procedure can be applied, research of the applicability of the various available aerodynamic models has to be performed. This is the first part of this paper, which focuses on the analysis of these models with respect to the goal function of required power dependent on the blade geometry for two flight conditions. After suitable models are identified, they are applied in in a variable fidelity optimization, which is benchmarked with a single fidelity optimization using the same optimization strategy.

2 AERODYNAMIC MODELS

One key discipline for the proper analysis of helicopter rotor blades is the modeling of the aerodynamics. However, as a regular helicopter blade is a slender wing with a high aspect ratio, the elastic effects are not negligible. On top of that, for a proper comparison of the performances between two rotors, the implicit constraint of a trimmed aircraft becomes necessary. To account for the elastic effects, as well as ensuring a proper trimmed condition, the comprehensive code HOST [7], majorly developed by Eurocopter, is used. HOST features a quasi 1D-beam elastic model extended from Bernoulli's theory. The trim procedure for static flight conditions, such as hover and cruise flight, is given by a Newton-Raphson method. As most comprehensive codes, HOST features some simple aerodynamics, but at the same time allows the coupling to more sophisticated methods, which are covered in the following.

2.1 Blade Element Theory

The idea of the blade element theory (BET) is to use look-up tables of the aerodynamic coefficients of the individual airfoil sections on the blade and then integrating them spanwise, as well as over azimuth. One major difficulty of the BET is the proper finding of the induced inflow angle, which is required to compute the sectional angle of attack. For hover flight, the BET can be extended with the momentum theory to produce more realistic results, while in forward flight generalized inflow models improve the aerodynamics. A detailed description is found in Leishman [22]. HOST features some semi-empirical corrections, mentioned in [13]. Nevertheless, even these improvements do not account for all physical phenomena, and particular 3D effects such as blade vortex interaction (BVI) are neglected or only semi-empirically modeled.

2.2 Finite State Inflow Models

HOST features a finite state inflow model (FISUW) developed by Basset et al. [26] which uses a modified accelerated potential theory to compute the inflow more realistically. The advantage of this approach compared to the classical inflow models is that the number of applied polynomials and harmonics can be set for the azimuthal and radial directions. The inflow velocity is determined by the forces on the blade, which are given from the look-up tables. Thus, an iterative procedure is applied to find an equilibrium between aerodynamic forces and the inflow velocities. Yet, FISUW is also not able to capture any BVI effects, but the downwash is accounted for more realistically.

2.3 Wake Vortex Modeling

There are two general variants of wake vortex modeling; prescribed and free. The principle is derived from the lifting line theory, where the bound circulation of the rotor is computed from the forces, which then yields the induced velocities. The difference between prescribed and free wake models is given by the description of the vortex field. While the prescribed model moves the vortices according to a semi-empirical definition, as done in the HOST module METAR [6], [13], a free wake model uses the induced velocities to move the wake filaments downstream, which results in a better representation of the wake. Latter approach has been implemented in the MESIR code by Michea [24]. The disadvantage of free wake models is that in practical applications they are less stable than prescribed wake models. In general, wake models allow the computation of BVI effects, but assume incompressible, inviscid and irrotational flow in the wake.

2.4 Panel Methods

At the DLR, a code called UPM is developed by Yin and Ahmed [36], which does not use airfoil polars to compute the loads, but a panel code, which allows the representation of the blade as a surface, rather than a line. The panel method is based upon the potential theory, which assumes incompressible, inviscid and irrotational flow, just as the vortex models. UPM itself includes an unsteady free wake model, which is coupled with the panel method. It is successfully applied to aero-acoustic problems in [35]. One strength of this approach is that BVI effects can be captured, while theoretically requiring less computational effort than CFD methods. Compressible effects are accounted for by Glauert's correction $(1/\sqrt{|M^2-1|})$ in UPM. A disadvantage of UPM is that it can not be coupled with HOST (yet), and thus elastic effects are neglected. However, a trim procedure is contained within UPM.

2.5 CFD

In this paper, CFD methods refer to the solution of the Euler and RANS equations using the FLOWer code [20] of the German Aerospace Center (DLR). The Euler equations neglect viscous effects, but are able to capture 3D effects, as well as compressible flows. Eventually the shock locations are not matched as well with Euler as with RANS. The RANS equations additionally account for viscous terms through a turbulence model. In this work the Wilcox $k-\omega$ turbulence model is used. For more details on the CFD setup, see Imiela [17]. The advantage of FLOWer coupled with a comprehensive code is that it yields high fidelity results [27], but is computationally expensive, and due to numerical viscosity added for stability, vortices tend to dissolve too fast and certain BVI aspects may not be modeled.

2.6 Comparison

Guided from the previous discussion, Table 5 in the appendix gives a concluding overview of the abilities and points out the weaknesses of each individual method. In this paper, these methods are categorized into low-, mid- and high fidelity methods based upon their theoretical abilities to model all physical effects of rotor aerodynamics properly. The BET and BET coupled with momentum theory (BEMT), generalized inflow models and finite state inflow models are categorized as low fidelity methods. These are usually suited for preliminary design as well flight mechanical considerations. Wake modeling with the BET or panel methods are mid-range fidelity, while solving the RANS equations is considered high fidelity. It has to be noted though, that even RANS has drawbacks. The numerical dissipation is still eminent, and turbulence modeling is not the best option for dynamic stall simulations. Other methods, such as vorticity transport models (VTM) [23], or further developed CFD methods like time-spectral and large or detached eddy simulations (LES/DES) [31] are not taken into account in this study.

3 INVESTIGATION OF AERODYNAMIC MODELS

The goal of the first part of this work is to identify suitable aerodynamic models to be applied later on for the variable fidelity optimization. Therefore, an investigation of the described models from Section 2 is performed with four different design parameters varied in two flight conditions. These parameters are taken from Imiela [18], namely tip twist for a linear twist distribution, tip chord tapering, horizontal and vertical offset of the tip, here synonymously used for anhedral and sweep. Fig. 1 depicts the design variables for clarity. The base line rotor is a 7A rotor [5] with $2.1m$ radius, and the beginning of the tip is set at $80.6\ \%$ rotor radius = $1.6926m$. In Table 1, the range and initial value of each parameter are summarized. The root chord length is adjusted to match a thrust equivalent weighted chord length of $c_{ref} = 0.14m$ when the tip chord length is modified. For a robust meshing procedure, the trailing edge is tapered, instead of a tap, which is featured by the original 7A rotor. As for the structural beam model, only the quarter chord position is adjusted, stiffness and inertia properties remain the same for all configurations.

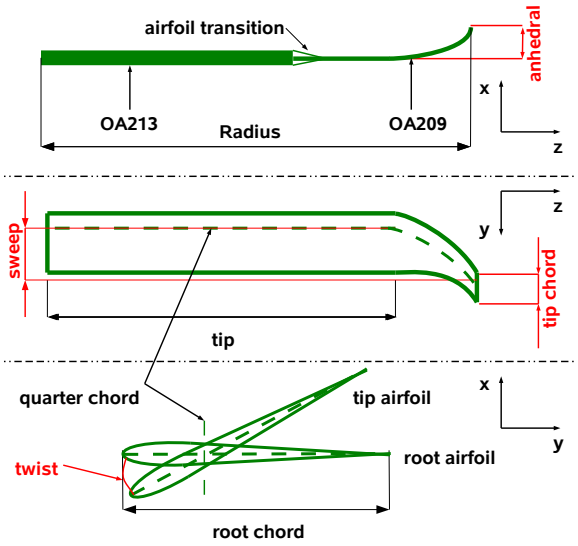

Figure 1: *The parameter anhedral, chord, sweep and twist for the modification of a 7A rotor.*

Parameter	baseline value	lower bound	upper bound
anhedral [$*c_{ref}$]	0.0	-1.0	1.0
tip chord [$*c_{ref}$]	1.0	0.5	1.5
sweep [$*c_{ref}$]	0.0	-1.0	1.0
twist [°]	-4.32	-20.0	0.0

Table 1: *parameter range. reference chord length* $c_{ref} = 0.14m$.

The two investigated flight conditions are hover and forward flight, both trimmed for a vertical force of $4400N$ with a tip Mach number of 0.646. In forward flight the advance ratio is $\mu = 0.38$ corresponding to a flight Mach number of 0.2468, while a virtual fuselage drag of $530N$ has to be overcome.

The investigation is organized as follows; at first the baseline rotor (7A) is computed, secondly a parameter variation study is performed, where each parameter is modified individually, and finally a genetic algorithm is applied to directly optimize on the different models to find the respective optima. The different models are designated as follows:

- BET: Computations based on the blade element theory. In forward flight the Pitt and Peters [29] generalized inflow model is used
- BEMT: BET coupled with the momentum theory, only valid for hover
- FISUW: BET coupled with a finite state inflow model
- PWAKE: BET coupled with a prescribed wake model
- FWAKE: BET coupled with a free wake model
- EU: Euler computations on a coarse mesh. In hover a periodic boundary condition is used, in forward flight only a single blade is modeled, thus neglected the effects of other blades.
- NS: Navier-Stokes computations. Just as EU, except with 15 points in the boundary layer included.
- FNS: Navier-Stokes computations on a fine mesh. In hover a periodic boundary condition is used, in forward flight a four-blade chimera setup is used.

In general, hover is considered quasi-steady, while forward flight is handled as an unsteady computation. FNS is considered the highest fidelity available, even though better models exist. For the specific details on the discretization of each method, check Table 6 in the appendix.

3.1 Baseline Rotor

The baseline rotor is computed for each individual method in hover and forward flight. Fig. 2 visualizes these results along with the results of the pure momentum theory denoted MT. The momentum theory defines the absolute possible minimum for the required power for any rotor of this radius, as it assumes inviscid, irrotational and incompressible flow of a stream tube.

In hover, the BEMT is in close agreement with the FNS computations, while the wake couple methods generally under predict the required power. The induced power from the FNS computation is $66.45kW$ in hover, which is mostly captured by the EU method. However, PM predicts a required power close to the required power given by the momentum theory. This is a questionable result, as the momentum theory assumes a constant inflow over the disc, which the 7A rotor does not have. The over prediction of required power of the NS method is attributed to the higher numerical dissipative nature of coarse meshes, and a roughly resolved boundary layer.

In forward flight, the FWAKE method is in close agreement with FNS. The prediction from the PM is

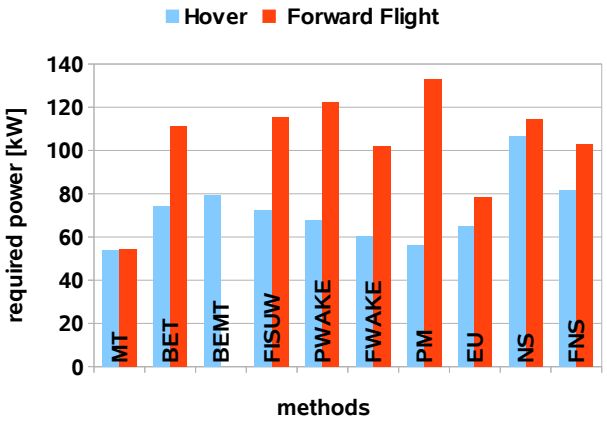

Figure 2: *Bar chart of the required power computed by each method for hover and forward flight.*

rather high. Reason for this is the lack of properly accounting for compressibility effects, as well as missing aero-elastic torsion, which is not modeled. This results in very high pitch control angles, leading to an increase in drag. The EU method computes about 20% less required power than FNS, which is in the range of the inviscid power computed by FNS, making it a valid result within the physical assumptions. The NS methods over predicts the power, just as it does in hover, for the same reasons; coarse dissipative grid and roughly resolved boundary layer. BET, FISUW and PWAKE over predict the required power. For the first two methods, this comes from the general methodology, while for PWAKE the prescribed wake does not match as well as a free wake, leading to an offset in power.

For the optimization process, in particular in the VF context, the right position of the optimum in the design space is important, not so much the absolute value. The assumption is that it can be computed afterwards with a high fidelity method in order to obtain the right absolute value. Thus, all future results concerning the goal function of required power, will be divided by the baseline value of the respective method and flight condition.

3.2 Sensitivity Study

The goal of the sensitivity study is to practically grasp the behavior of the goal function with respect to geometry changes. Fig. 4 to Fig. 11 depict the parameter variations in hover and forward flight with the legend given in Fig. 3. At a first glance at these figures one can see that similar methods, BET, BEMT, FISUW, or PWAKE, FWAKE, or PM, or EU, NS, FNS, yield similar tendencies of parameter preference stemming from the similarity in their physical assumptions. Most trends of FNS are captured by EU fairly well, which in turn means that for these goal functions viscous effects are of minor importance. This statement may not be valid when an airfoil optimization is in-

cluded.

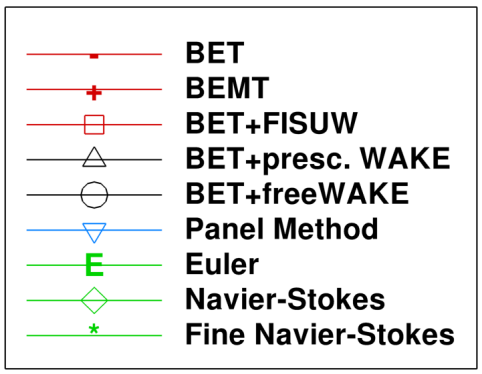

Figure 3: *Legend for the sensitivity figures.*

In hover, the results are widespread. The anhedral parameter (Fig. 4) only seems to have an effect on the structure when using low fidelity methods (BET, BEMT, FISUW), while wake coupled methods capture a different trend, as the CFD methods. The optimum of the anhedral parameter for the wake models lies at -1 with a power reduction to 82% and 75% for PWAKE and FWAKE respectively, but is intentionally not plotted in Fig. 4. The benefits of an anhedral or dihedral in hover are greater than in forward flight (Fig. 5), where the slight aerodynamic gain is lost due to the aeroelastic effects. Points beyond an absolute value of 0.3 anhedral are not convergeable for some methods, as seen in the Fig. 5.

The trend of the tip chord parameter (Fig. 6, Fig. 7), which tapers the blade, is captured similarly for all methods, and flight conditions. As it offloads the blade on the outboard tip, the induced velocity is reduced, as well as the viscous drag, if modeled, at the tip, which has the greatest moment arm.

Blade sweep (Fig. 8, Fig. 9) brings an improvement of the goal function for all methods and flight conditions. In hover flight, two optima exist for BET, FISUW and the CFD methods; a forward swept blade is slightly more favorable than a backward swept blade for EU and FNS. For all other methods, backward sweep is perceived more valuable. In forward flight, due to strong blade torsion at the tip, only backward sweep is advantageous. Some values can not be computed, as trimming the blade proofs to be impossible. The PM method, as a result of missing elastic modeling, leads to an infeasible preference of forward sweep in forward flight.

A parabola like curve is given for the twist parameter (Fig. 10, Fig. 11) for all methods in both flight conditions. Yet, the position of the minimum varies across the methods. The low fidelity methods usually have this optimum at low angles, while with increasing fidelity this value rises. However, EU and NS predict a greater twist angle than FNS. This arises from the coarse mesh, where more numerical dissipation is given.

Overall, it is noticed that the wake coupled methods show stronger trends of all parameters than the other methods. For example the effect on the anhedral parameter in hover grants an improvement of over 19% for PWAKE and over 21% for FWAKE. For FWAKE this leads to an absolute value for the required power of $45.3kW$ in hover, which is below the theoretical value of $54.1kW$. Results from these methods should thus be looked upon with skepticism, and are reasons to exclude these models for hover optimizations.

Concluding from this sensitivity study, the downwash is the main driver for the hover case seen from the effect of blade twist, while the lift redistribution towards the inboard rotor caused by the blade sweeping and tapering brings the most improvement in forward flight.

3.3 Direct Optimization

In order to identify suitable models for a variable fidelity rotor optimization, a direct optimization using the genetic algorithm SOGA [12] in the Dakota Toolbox is performed for each aerodynamic model and both flight cases. The advantage of using a genetic algorithm is that the likelihood of finding a globally valid optimum is high, yet the major drawback is that it is very resource consuming and the local accuracy is limited. The criteria for selecting the various methods is based upon their robustness, physical feasible representation of the required power and the computational time required to execute the simulation. An exception is made for the four-bladed Chimera computation in forward flight using RANS, for which the optimum is found through the single fidelity optimization described in Section 4, as direct optimization is too costly.

3.3.1 Hover

In Table 2, the metrics for the final rotor of each hover optimization is listed. The column featuring FNS shows the value of this individual rotor configuration, when it is re-computed with FNS. The idea is to see how much the optima correspond with each other. In order to visualize these various parameters, the different blade configurations are shown in Fig. 15. The gain of the anhedral parameter is not captured by the low fidelity methods. The wake coupled methods all do prefer an anhedral, while the CFD methods tend to a dihedral. NS does not go for such a high value of dihedral, given the fact that the tip vortex dissipates faster on the coarse mesh. The EU method has a similar trend as FNS, as it is possible to tune out the numerical dissipation more than for NS. This leads to instabilities with rotors for which transonic effects occur in hover, yet these are non-optimal configurations at the

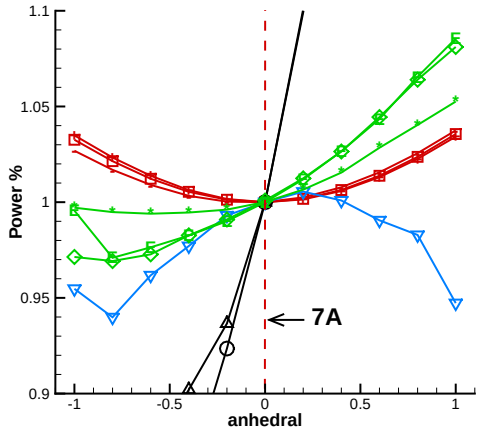

Figure 4: *anhedral variation in hover.*

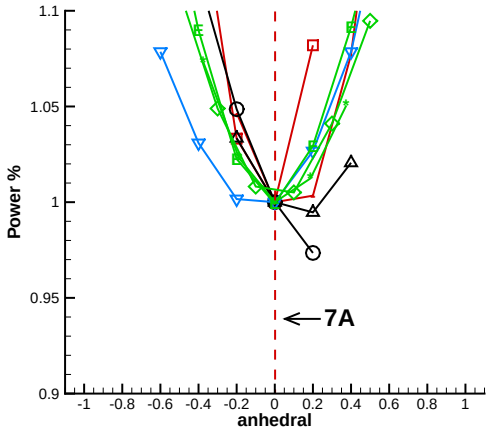

Figure 5: *anhedral variation in forward flight.*

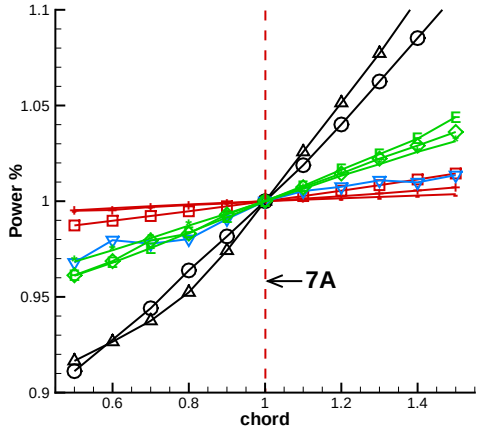

Figure 6: *chord variation in hover.*

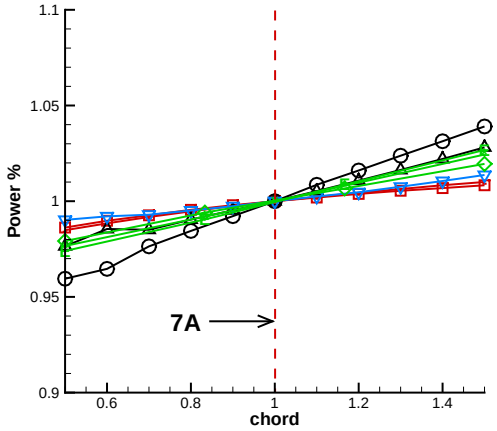

Figure 7: *chord variation in forward flight.*

same time and thus are left out of consideration for the optimizer. All methods except FWAKE yield a tapered tip, which corresponds to the findings of the sensitivity study. From the different behavior of the sweep parameter, one can see that backward or forward sweeping of the blade depends on the method. From investigating single individuals of the FNS optimization, it is found that the required power is a multi-modal function given from forward and backward sweeping. For the twist parameter, a similar finding to the one given by the sensitivity study is made; with increasing fidelity the tip twist angle grows larger, except for FWAKE. The final angle is somewhat larger for EU and NS than FNS, yet not too far off.

An intermediate conclusion from these results is that the simple low fidelity methods are not appropriate for optimizing anhedral, and the twist parameter is too low. The wake coupled methods (PWAKE,FWAKE and PM) are sometimes unstable in their prediction, in particular FWAKE. The final rotor configurations yield

Method	Power	anh.	chord	sweep	twist	FNS
BET	0.986	-0.05	0.89	0.97	-1.74	1.003
BEMT	0.988	0.39	0.60	0.83	-5.97	0.976
FISUW	0.979	-0.04	0.61	0.97	-5.48	0.963
PWAKE	0.749	-0.99	0.62	-0.74	-9.16	0.959
FWAKE	0.337	-0.98	1.41	-0.99	-2.56	1.045
PM	0.767	-1.00	0.89	0.69	-9.43	0.980
EU	0.879	0.98	0.64	-0.95	-16.52	0.933
NS	0.898	0.25	0.63	-0.97	-16.52	0.938
FNS	0.917	0.76	0.54	-0.97	-12.34	0.917

Table 2: *Final results of the different optimization in hover.*

power requirements close to or even below the theoretical minimum, which is suspicious. The group of CFD results agree mostly with each other. However, it should be kept in mind that numerical dissipation has a great impact on the tip vortex and thus on the anhedral parameter, as seen with NS in contrast to EU and FNS. Given these findings, the proposed methods for hover optimization in a VFM framework are listed

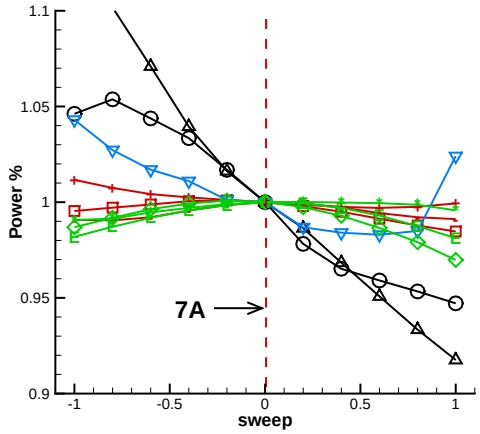

Figure 8: *sweep variation in hover.*

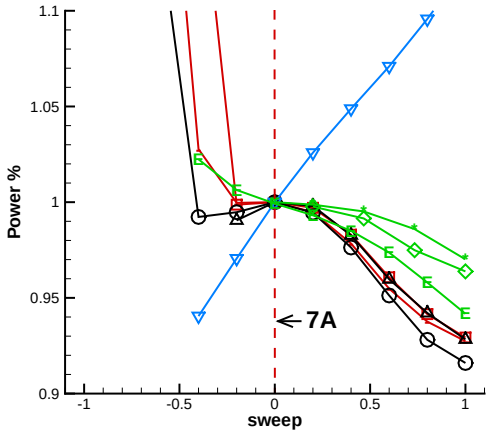

Figure 9: *sweep variation in forward flight.*

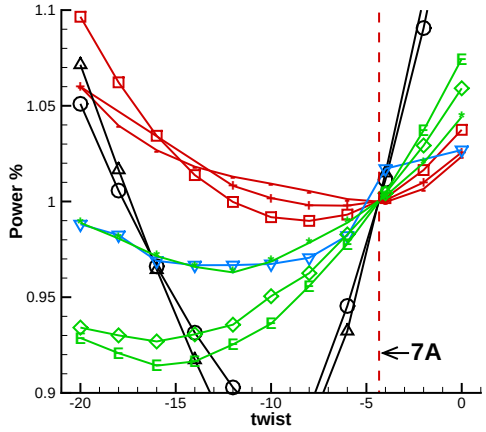

Figure 10: *twist variation in hover.*

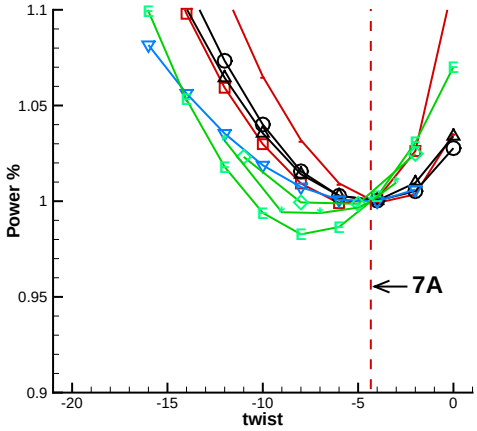

Figure 11: *twist variation in forward flight.*

on the left side of Table 4.

3.3.2 Forward Flight

In a similar fashion to the hover case, Table 3 summarizes the findings from the forward flight optimization with the blades depicted in Fig. 16. In forward flight, the results are more in harmony than in hover. BET, FISUW and PM are misleading in terms of the chord parameter, for which the optimization process features a widening of the blade towards the tip. Furthermore, PM features an optimum analog to the hover optimum seen from the preference for anhedral given the lack of structural modeling. The other solutions indicate no strong favoring of dihedral, a full backward sweep, and a tip twist slightly greater than the baseline.

Deducting from these observations, the available (low fidelity) tools for computing rotor blades are more suitable for (fast) forward flight optimizations than for hover optimizations. For forward flight, a suitable combination of methods for a VF framework given on the right side of Table 4. The prescribed wake is favored over the free wake model, as it proofed to be more robust, and required a fraction of the computational effort.

Method	Power	anh.	chord	sweep	twist	FNS
BET	0.926	0.25	1.18	0.95	-5.48	0.989
FISUW	0.866	0.25	1.46	0.86	-5.48	1.009
PWAKE	0.928	-0.01	0.57	0.94	-4.52	0.952
FWAKE	0.868	0.25	0.69	0.86	-7.70	0.957
PM	0.577	-0.99	1.48	-0.58	-2.61	1.380
EU	0.904	-0.01	0.84	0.97	-5.48	0.968
NS	0.985	-0.04	0.70	0.86	-4.13	0.964
FNS	0.941	0.10	0.50	1.00	-5.34	0.941

Table 3: *Final results of the different optimizations in forward flight.*

Fidelity	**hover**	**forward flight**
low	FISUW 8 cpus	PWAKE 1 cpum
mid	EU 5 cpuh ≈ 2,250 FISUW	EU 75 cpuh ≈ 4,500 PWAKE
high	FNS 160 cpuh ≈ 32 EU ≈ 72,000 FISUW	FNS 2600 cpuh ≈ 35 EU ≈ 157,500 PWAKE

Table 4: *Choices of low-,mid and high fidelity for each flight condition and their CPU times. (cpus=cpu seconds, cpum=cpu minutes, cpuh=cpu hours)*

4 OPTIMIZATION FRAMEWORK.

In order to take advantage of the findings of the previous section, a framework for VF optimization is developed. It features a similar approach as a regular surrogate based optimization (SBO) framework as explained in depth in [2], or [11]. For completeness, the VFM process is sketched in Fig. 12. A design of experiments (DoE) for high and low fidelity data is performed to gather the initial samples required for creating the surrogate model. Optionally, the low fidelity optimum is found and this point is sampled in the high fidelity DoE. After the VF surrogate model is created, an iterative loop is started, where the design with the highest expected improvement is searched and computed with the HF simulation. The obtained result is inserted into the surrogate model and the loop is started over until the optimization is finished.

Opposing to the Co-Kriging methodology applied in [3] and [34], this VF Kriging method is inspired by Hierarchical Kriging seen in [15] and [33]. The low fidelity model is built from a single fidelity Kriging of an arbitrary polynomial for the trend function:

$$\hat{f}_{LFM}(\vec{x}) = \vec{f}_v(\vec{x})^T \vec{\beta}_{LFM} + \epsilon_{LFM}(\vec{x}) \quad (1)$$

where $\hat{f}$ is the predictor value, $\vec{x}$ the design vector, $\vec{f}_v$ the polynomials, $\vec{\beta}$ the polynomial coefficients and ϵ the error modeled by the Gaussian process. For the Hierarchical Kriging model, the polynomial trend is exchanged with the low fidelity model:

$$\hat{f}_{HFM}(\vec{x}) = \hat{f}_{LFM}(\vec{x})\rho + \vec{x}^T \vec{\beta}_{HFM} + \epsilon_{HFM}(\vec{x}) \quad (2)$$

This way, the low fidelity model $\hat{f}_{LFM}$ is included by a scaling parameter ρ, and a first order bridge function is given by $\vec{x}^T\vec{\beta}$. Here, for the regular Kriging the polynomial order is set to two. If the amount of sampled points is insufficient for determining all coefficients, the polynomial order is reduced, while for the Hierarchical Kriging the bridge is removed.

The strategy for finding the optimum in the surrogate model is simplified by running a full factorial DoE with eight samples in each spatial direction, and starting the local searcher by Hooke and Jeeves [16] from the best point found. This is somewhat a brute force method and is only considered feasible for this small number of parameters of four, and should not be used for more parameters. The method is also applied for tuning the hyper parameters of the Kriging model, which optimize the concentrated likelihood function.

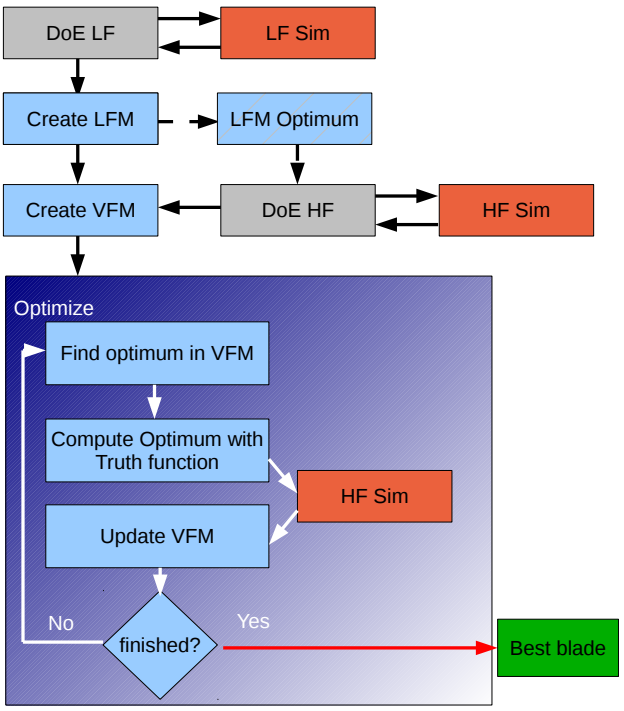

Figure 12: *VFM Framework for the fusion of low (LFM) and high (HFM) fidelity methods.*

5 SURROGATE BASED OPTIMIZATION

In this section the optimization framework is applied based on a low and a mid-fidelity method. The low to mid fidelity optimization is considered more difficult as the trend function is further away than for the mid to high fidelity optimization. For this test, several initial sampling strategies are used.

The point sampling starts the update process with only one selected point in the DoE. For single fidelity optimization using the mid-fidelity method only, this point is the 7A rotor, while for variable fidelity optimization, the best low fidelity optimum is used, as predicted by the low fidelity surrogate model.

The hyper cross sampling additionally computes neighboring points left- and right of the optimum for each direction of the design space similar to finite differences.

For comparison with Monte-Carlo samplings, ten central voronoi tessellated (CVT) cubes [21] are generated containing 12 samples each.

The DoE for the low fidelity model is a full factorial cube with four samples in each direction, leading to 256 samples in total.

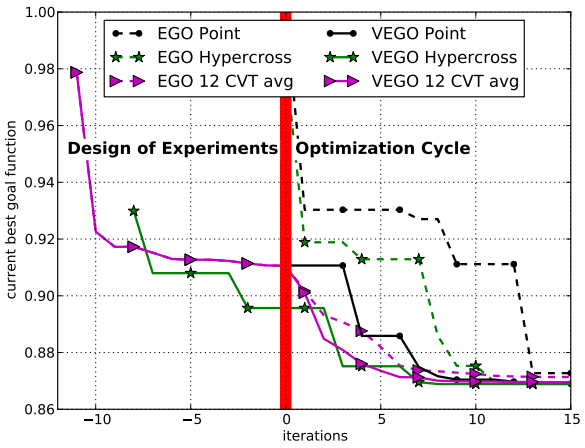

Figure 13: *Comparison single (EGO) and variable fidelity (VEGO) optimization in hover.*

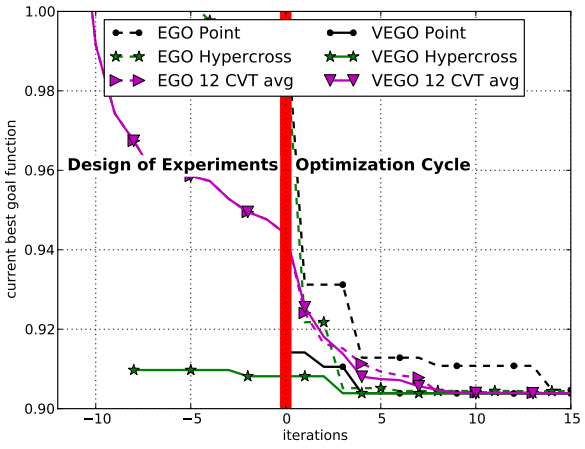

Figure 14: *Comparison single (EGO) and variable fidelity (VEGO) optimization in forward flight.*

Fig. 13 and Fig. 14 graph the best goal function value sampled so far over the current iteration in the process for hover and forward flight optimizations, respectively. The single fidelity SBO is marked EGO in the merit of the optimizer developed by Jones et. al [11], while the variable fidelity SBO is referred to as VEGO (Variable fidelity EGO). The first iteration represents the first update sample, while all previous iterations belong to the DoE. The graphs might descent before an actually optimization takes place, because some points in the DoE might already be better than others.

In hover, the gain from the variable fidelity approach is less than in forward flight likely due to the more complex goal function and the greater difference between the low- an mid fidelity model. Still, for both flight cases, it is understood that the variable fidelity optimization is better when the deterministic samplings of a point and hyper cross around the low fidelity optimum are used. In hover, the random 12 point CVT sampling reduces the number of optimization cycles, as the function is more complex than in forward flight. However, for the random 12 point CVT sampling, the superiority of variable to single fidelity vanishes. Reason for this is the saturation of information with increasing number of samples. The single fidelity model, based upon pure Kriging, is more flexible as it can adjust the polynomials of the trend model. For Hierarchical Kriging, the trend function cannot be tweaked as much, as it is fixed by the low fidelity model.

Nevertheless, for a small number of parameters and a rare amount of samples the variable fidelity approach succeeds for both flight conditions. The point sampling yields the smallest total required number of computations for single as well as variable fidelity optimizations. Comparing the required resources, 69.2% in hover and 35.2% in forward flight of the mid-fidelity samples are required to reach the optimum in contrast to the single fidelity optimizations. As for the accuracy of the results, the optimal configurations obtained from the individual runs are in harmony with the ones from the direct optimization from Section 3.3. They are slightly better by less than 2% for all cases and in the same region of the design parameters.

6 CONCLUSIONS

An investigation containing a range of computational methods for rotor aerodynamics ranging from the blade element theory to computational fluid dynamics has been performed. The focus was on the analysis of the required power with respect to geometry changes of the rotor blades. Therefore, the 7A rotor has been computed for all methods as a reference solution. Following that, a sensitivity analysis, as well as an optimization using a genetic optimizer have been performed, to see which method best finds the trend of the high fidelity model.

In hover, the anhedral parameter was perceived very differently, while chord tapering and sweep had similar behavior among the methods. The twist parameter followed a similar trend, yet the optimal location varied strongly across the methods.

The agreement of these parameters was generally better in forward flight across the various methods. Only the panel method, which did not include elastic deformations, yielded questionable results. The plain blade element theory, as well as the finite state inflow model did not taper the chord in the full optimization. Optimizations with the other methods returned similar blades with similar performances.

Concluding from this investigation low, mid and high fidelity models have been selected for the hover and the forward flight case. For hover these models are a finite state inflow model, Euler CFD computations on a coarse mesh, and Navier-Stokes computations on a fine grid. Opposing to this, a prescribed wake model, single blade Euler computations on a coarse mesh, and a four-bladed Chimera setup using the Navier-Stokes equations are selected for forward flight optimization. While in forward flight a single optimum exists which is in compliance with most methods, in hover at least two optima exist, which also vary across the models. This makes hover a more difficult case in terms of optimization.

A variable fidelity framework based on Hierarchical Kriging has been designed and tested for the same four parameters from the initial investigation using low and mid fidelity methods. For both approaches, variable as well as single fidelity optimizations, it was seen that starting only with one initial sample and proceeding with sampling the expected improvement in the surrogate yielded the least amount of samples required in total. The variable fidelity approach helps to reduce the required computational resources through the decrease of high fidelity computations to 69.2% and 35.2% in hover and forward flight, respectively. The greater reduction in forward flight is explained with the less complex goal function. An effect of surrogate model saturation has been seen, where single and variable fidelity models become equally good for an increasing number of initial samples. No advantage from variable to single fidelity is seen for the initial random 12 point sampling, independent of the flight condition.

7 OUTLOOK

Currently the mid-high fidelity optimization is underway, and is expected to work better than low-mid fidelity optimizations. Future work will include a broader range of design parameters, as well as constraint multi-objective optimizations.

References

[1] J. Peter A. Dumont, A. Le Pape and S. Huberson. Aerodynamic shape optimization of hovering rotors using a discrete adjoint of the reynolds-averaged navier-stokes equations. *Journal of American Helicopter Society*, 56:032002–1–11, 2011.

[2] A. Sòbester A. Forrester and A. Keane. *Engineering Design via Surrogate Modelling - A Practical Guide*. John Wiley & Sons Ltd., 2008.

[3] A. Sòbester A. I.J Forrester and A. J Keane. Multi-fidelity optimization via surrogate modelling. *The Royal Society*, 463:3251–3269, 2007.

[4] A. D'Andrea A. Massaro and E. Benini. Multiobjective-multipoint rotor blade optimization in forward flight conditions using surrogate-assisted memetic algorithms. In *37th European Rotorcraft Forum*, 2011.

[5] M. Allongue and J.P. Drevet. New rotor test rig in the large modane wind tunnel. In *European Rotorcraft Forum*, 1989.

[6] G. Arnaud and P.Beaumier. Validation of r85/metar on the puma rae flight tests. In *18th European Rotorcraft Forum*, 1992.

[7] K. Kampa W. von Grünhagen-P.-M. Basset B. Benoit, A.-M. Dequin and B. Gimonet. Host, a general helicopter simulation tool for germany and france. In *American Helicopter Society 56th Annual Forum, Virginia Beach, Virginia, May 2-4, 2000*, 2000.

[8] P. P. Friedmann B. Glaz and L. Liu. Surrogate based optimization of helicopter rotor blades for vibration reduction in forward flight. In *47th AIAA/ASME/ASCE/AHS/ASC Structures, Structural Dynamics, and Materials Conference 1 - 4 May 2006, Newport, Rhode Island*, 2006.

[9] K. B. Collins. *A Multi-Fidelity Framework for Physics Based Rotor Blade Simulation and Optimization*. PhD thesis, Georgia Institute of Technology, 2008.

[10] C.S.Johnson and G.N.Barakos. Optimising aspects of rotor blades in forward flight. In *49th AIAA Aerospace Sciences Meeting*, 2011.

[11] M. Schonlau D. R. Jones and W. J. Welch. Efficient global optimization of expensive black-box functions. *Journal of Global Optimization*, 13:455–492, 1998.

[12] J. Eddy. Effective generation of paretos sets using genetic programming. In *ASME 2001 Design Engineering Technical Conferences*, 2001.

[13] B. Benoit G. Arnaud and F. Toulmay. Improvements to the aerodynamic model of the r85 helicopter rotor code: Validation and applications. In *28th ISL Applied Aerodynamics Symposium*, 1991.

[14] R. Ganguli. Survey of recent developments in rotorcraft design optimization. *Journal of Aircraft*, 41, No. 3:493–510, 2004.

[15] Z.-H. Han and S. Görtz. A hierarchical kriging model for variable-fidelity surrogate modeling. *To be published in AIAA Journal*, X:Y, 2012.

[16] R. Hooke and T. A.Jeeves. Direct search solution of numerical and statistical problems. *Journal of Assosication of Computing Machinery*, 8:212–229, April 1961.

[17] M. Imiela. High-fidelity optimization framework for helicopter rotors. *Aerospace Science and Technology*, (0):–, 2011.

[18] M. Imiela. *Mehrpunktoptimierung eines Hubschrauberrotors im Schwebe- und Vorwärtsflug unter Berücksichtigung der Fluid-Struktur-Wechselwirkung*. PhD thesis, Institut für Aerodynamik und Strömungstechnik Braunschweig, 2012.

[19] R. Ganguli K. K. Saijal and S. R. Viswamurthy. Optimization of helicopter rotor using polynomial and neural network metamodels. *Journal of Aircraft*, 48-2:553–566, 2011.

[20] Aumann P. Bartelheimer W. Bleecke H. Eisfeld B.-Fassbender-J. Kuntz M. Lieser J. Monsen E. Heinrich R. Mauss M. Raddatz J. Reisch U. Roll B. Schwarz T. Kroll, N. Flower installation and user handbook, release 116. Technical report, German Aerospace Center (DLR), 2008.

[21] Q. Du L. Ju and M. Gunzburger. Probabilistic methods for centroidal voronoi tessellations and their parallel implementations. *Parallel Computing*, 28:1477–1500, 2002.

[22] J.G. Leishman. *Principles of Helicopter Aerodynamics*. Cambridge University Press, 2006.

[23] K. Duraisamy M. E. Kelly and R. E. Brown. Predicting blade vortex interaction, airloads and acoustics using the vorticity transport model. In *AHS Specialists' Conference on Aeromechanics*, 2008.

[24] B. Michea. *Etude des Sillages de Rotors D'Helicoptere en Vol D'Avancement et de leur Influence sur les Performances du Rotor. (Interaction Pale-Tourbillon)*. PhD thesis, Universite Paris 6, 1992.

[25] A. I. Azamatov J.-W. Lee N. A. Vu, H.-J. Kang and Y.-H. Byun. Aerodynamic design optimization of helicopter rotor blades in hover performance using advanced configuration generation method. In *35th European Rotorcraft Forum 2009*, 2009.

[26] J.V.R. Prasad P.-M. Basset, O. Heuze and M. Hamers. Finite state rotor induced flow model for interferences and ground effect. In *American Helicopter Society 57th Annual Forum*, 2001.

[27] K. Pahlke and B. G. van der Wall. Chimera simulations of multibladed rotors in high-speed forward flight with weak fluid-structure-coupling. *Aerospace Science and Technology*, 9:379–389, 2005.

[28] A.. Le Pape and P. Beaumier. Numerical optimization of helicopter rotor aerodynamic performance in hover. *Aerospace Science and Technology*, 9:191–201, 2005.

[29] D.M. Pitt and D.A. Peters. Theoretical prediction of dynamic inflow derivatives. *Vertica*, 5:21–34, 1981.

[30] C. Yang T. Aoyama S. Jeong S. Chae, K. Yee and S. Obayashi. Helicopter rotor shape optimization for the improvement of aeroacoustic performance in hover. *Journal of Aircraft*, 47-5:1170–1783, 2010.

[31] E v.d. Weide J. Sitaraman S. Choi, J. J. Alonso. Validation study of aerodynamic analysis tools for design optimization of helicopter rotors. In *25th AIAA Applied Aerodynamics Conference*, 2007.

[32] K. Lee G. Iaccarino S. Choi, M. Potsdam and J. J. Alonso. Helicopter rotor design using a time-spectral and adjoint-based method. In *12th AIAA/ISSMO Multidisciplinary Analysis and Optimization Conference 10 - 12 September 2008, Victoria, British Columbia Canada*, 2008.

[33] W. Chen Y. Xiong and K.-L. Tsui. A new variable-fidelity optimization framework based on model fusion and objective-oriented sequential sampling. *Journal of Mechanical Design*, 130(11):111401, 2008.

[34] W. Yamazaki and D. J. Mavripilis. Derivative-enhanced variable fidelity surrogate modeling for aerodynamic functions. In *AIAA - Aerospace Sciences Meeting and Exhibit*, 2011.

[35] J. Yin and A. Stürmer. Noise radiation from installed pusher propeller using coupling of unsteady panel method, actuator disk and fw-h methodology. In *16th AIAA/CEAS Aeroacoustics Conference, Stockholm*, 2010.

[36] J.P. Yin and S.R. Ahmed. Treatment of unsteady rotor aerodynamics using a 3-d panel method. Technical report, Deutsche Forschungsantalt für Luft- und Raumfahrt Forschungsbereich Strömungsmechanik, 1994.

8 APPENDIX

Fidelity	**Low**			**Mid**			**Mid-High**	**High**
Methods	BET	BEMT	BET & finte state inflow	BET & presc. wake model	BET & free wake	Panel Method & free wake	Euler	RANS
boundary layer/ friction	TD ⊙-⊕	TD ⊙-⊕	TD ⊙-⊕	TD ⊙-⊕	TD ⊙-⊕	N/A ⊖	N/A ⊖	viscousity turb.model ⊕
compressible flow	TD ⊙	TD ⊙	TD ⊖-⊙	TD ⊖-⊙	TD ⊖-⊙	CF ⊖	S ⊕	S ⊕⊕
laminar-turb. transition	TD ⊙	TD ⊙	TD ⊖-⊙	TD ⊖-⊙	TD ⊖-⊙	N/A ⊖	N/A ⊖	N/A ⊖
stall	TD ⊕	TD ⊕	TD ⊙-⊕	TD ⊙	TD ⊙	N/A ⊖	S ⊖	S ⊕
downwash	CF ⊖	momentum theory ⊙	CF VF ⊙	CF VF ⊙-⊕	CF VF ⊕	S ⊕	S ⊕	S ⊕⊕
3D effects	CF ⊖	CF ⊙	CF VF ⊖-⊙	CF VF ⊙-⊕	CF VF ⊙-⊕	S ⊕	S ⊕	S num. damping ⊕

Table 5: *Methods as implemented in comparison with different aerodynamic effects. Legend: CF- corrections factors, S- complete field solution, VF- velocity field, TD- tabled data; ⊖- poor/no, ⊙- fair, ⊕- good, ⊕⊕- very good prediction capabilites.*

case	**hover**		**forward flight**	
locations	radial	chord	radial	chord
BET	31	1	31	1
BEMT	31	-	31	-
FISUW	31	-	31	-
PWAKE	25	1	25	1
FWAKE	25	1	2	1
PM	15	31	15	31
EU	25	61	32	96
	197,142 cells		380,016 cells	
NS	25	61	32	96
	251,526 cells		589,680 cells	
FNS	61	201	64	193
	2,266,236 cells		17,478,960 cells	

Table 6: *Discretization of the blade for the individual solvers and flight conditions.*

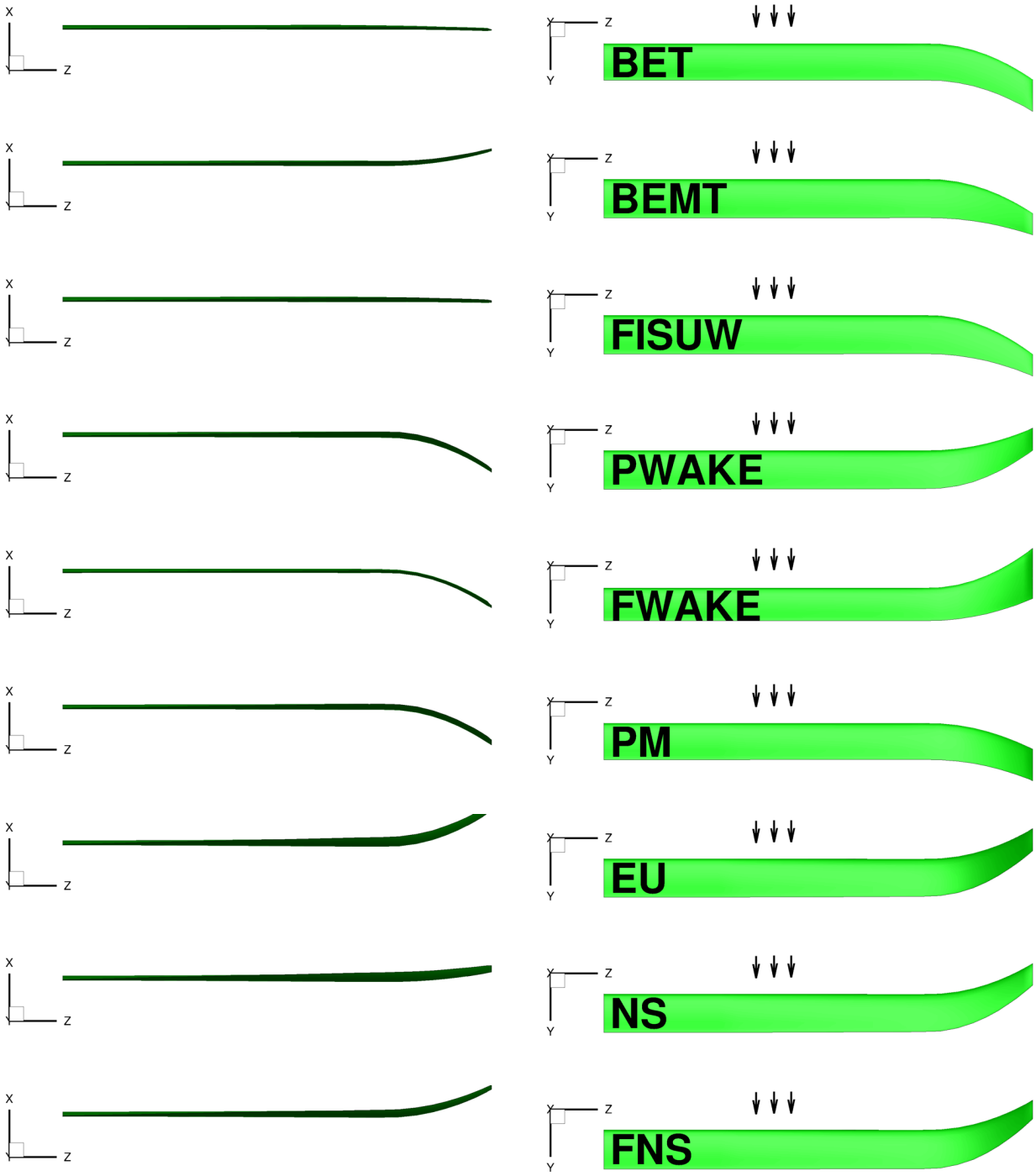

Figure 15: *Best blades of the different optimizations in hover.*

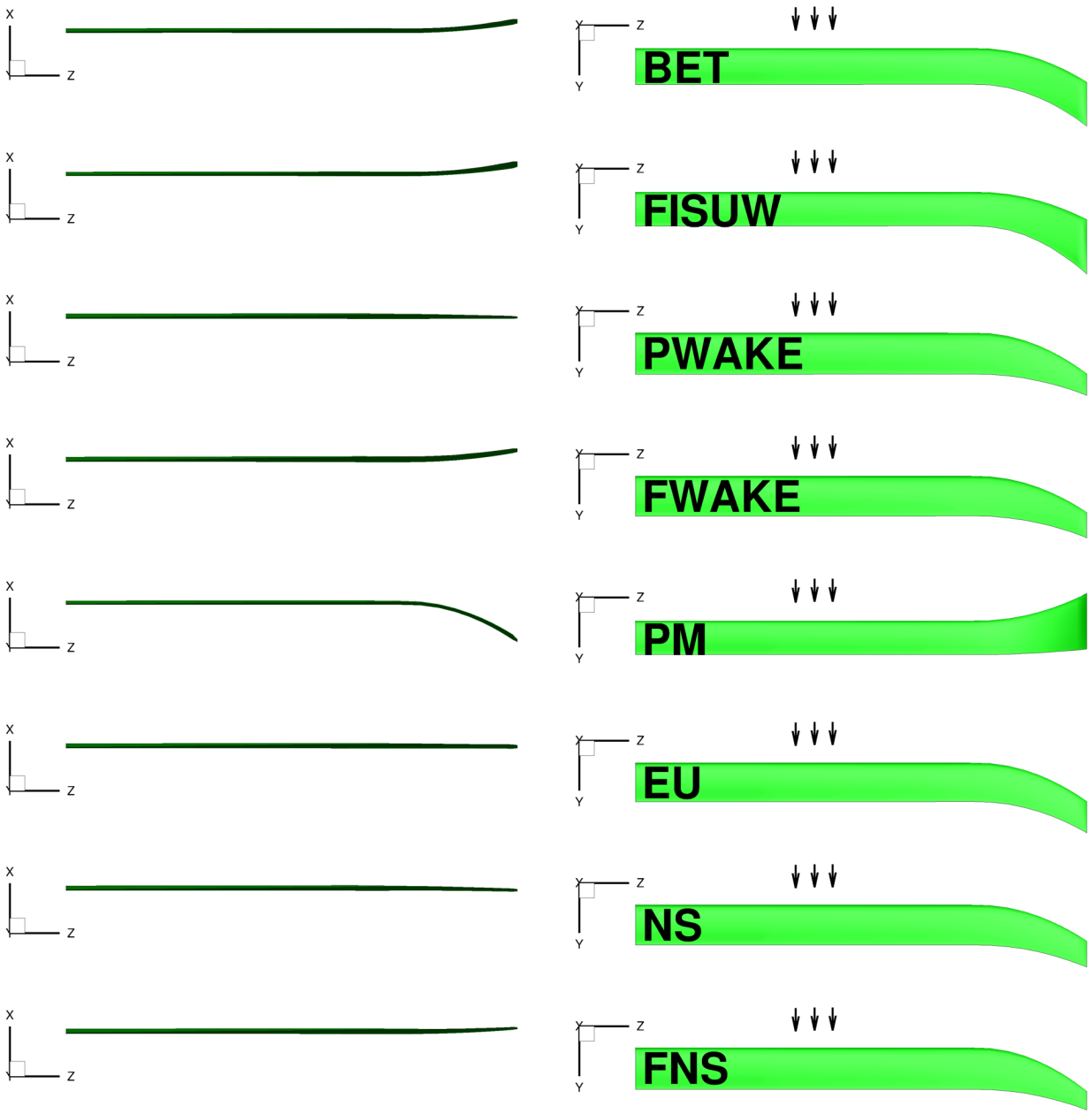

Figure 16: *Best blades of the different optimizations in forward flight.*